The formin mDia2 stabilizes microtubules independently of its actin nucleation activity

Francesca Bartolini,[1] James B. Moseley,[2] Jan Schmoranzer,[1] Lynne Cassimeris,[3] Bruce L. Goode,[2] and Gregg G. Gundersen[1]

[1]Department of Pathology, Anatomy and Cell Biology, Columbia University, New York, NY 10032
[2]Department of Biology and Rosenstiel Basic Medical Sciences Research Center, Brandeis University, Waltham, MA 02454
[3]Department of Biological Sciences, Lehigh University, Bethlehem, PA 18015

A critical microtubule (MT) polarization event in cell migration is the Rho/mDia-dependent stabilization of a subset of MTs oriented toward the direction of migration. Although mDia nucleates actin filaments, it is unclear whether this or a separate activity of mDia underlies MT stabilization. We generated two actin mutants (K853A and I704A) in a constitutively active version of mDia2 containing formin homology domains 1 and 2 (FH1FH2) and found that they still induced stable MTs and bound to the MT TIP proteins EB1 and APC, which have also been implicated in MT stabilization. A dimerization-impaired mutant of mDia2 (W630A) also generated stable MTs in cells. We examined whether FH1FH2mDia2 had direct activity on MTs in vitro and found that it bound directly to MTs, stabilized MTs against cold- and dilution-induced disassembly, and reduced the rates of growth and shortening during MT assembly and disassembly, respectively. These results indicate that mDia2 has a novel MT stabilization activity that is separate from its actin nucleation activity.

Introduction

Formins are a family of ubiquitous, conserved proteins that are implicated in a wide range of actin-based processes, such as cell polarization, cytokinesis, and cell morphogenesis. Formins are defined by their signature formin homology (FH) 2 domain, which assembles unbranched actin structures from the barbed ends (Pruyne et al., 2002; Sagot et al., 2002). The FH2 domain forms a tethered dimer consisting of two antiparallel elongated actin binding domains (Shimada et al., 2004; Xu et al., 2004). Mutation of conserved tryptophans at the dimerization interface abrogates actin assembly activity, suggesting that the dimer is the functional state of formin proteins (Moseley et al., 2004; Xu et al., 2004). Adjacent to the FH2 domain is a proline-rich FH1 domain that can accelerate the rate of filament elongation through interactions with profilin-bound actin monomers (Sagot et al., 2002; Kovar et al., 2003, 2006; Li and Higgs, 2003; Pring et al., 2003; Moseley et al., 2004; Romero et al., 2004; Vavylonis et al., 2006).

Correspondence to Gregg G. Gundersen: ggg1@columbia.edu

J.B. Moseley's present address is Laboratory of Yeast Genetics and Cell Biology, The Rockefeller University, New York, NY 10021.

Abbreviations used in this paper: DAD, diaphanous autoregulatory domain; DIC, differential interference contrast; DRF, Diaphanous-related formin; FH, formin homology; GBD, GTPase binding domain; LPA, lysophosphatidic acid; MT, microtubule; TIRF, total internal reflection fluorescence.

The online version of this paper contains supplemental material.

Diaphanous-related formins (DRFs) include Dia (diaphanous), DAAM (disheveled-associated activators of morphogenesis), and FRL (formin-related proteins identified in leucocytes) in mammals and Bni1 and Bnr1 in yeast (Higgs and Peterson, 2005; Rivero et al., 2005). The DRF subfamily is characterized by domains that regulate the subcellular localization and formin activation by Rho family GTPases. The binding of Rho-GTP to the GTPase binding domain (GBD) is thought to activate DRFs by relieving an autoinhibitory interaction between the adjacent N-terminal diaphanous inhibitory domain and a short segment located on the C-terminal side of the FH2 domain, the diaphanous autoregulatory domain (DAD; Watanabe et al., 1999; Alberts, 2001; Li and Higgs, 2005; Otomo et al., 2005; Rose et al., 2005). Functional consequences of DRF activation generally depend on the ability of DRFs to nucleate actin polymerization, resulting in the formation of linear actin filaments such as actin cables in yeast or actin fibers and filopodia in higher eukaryotes. Cellular functions mediated by DRFs include both cytoskeletal rearrangements and transcriptional activation of specific promoters such as the serum response element (Copeland and Treisman, 2002). DRF's ability to remodel the actin cytoskeleton has been implicated in cytokinesis, tissue morphogenesis, cell polarity, and cell adhesion, where they appear to be required for filopodia formation, focal adhesion turnover, and, more recently,

The Rockefeller University Press $30.00
J. Cell Biol. Vol. 181 No. 3 523–536
www.jcb.org/cgi/doi/10.1083/jcb.200709029

T cell proliferation and migration (Eisenmann et al., 2007; Goode and Eck, 2007; Gupton et al., 2007; Sakata et al., 2007). Two members of the Dia family in mouse (mDia1 and mDia2) also regulate endocytosis and endosome trafficking, presumably by promoting endosome actin coat formation and dynamics (Tominaga et al., 2000; Gasman et al., 2003; Fernandez-Borja et al., 2005; Wallar et al., 2007).

There is growing evidence that formins may also be involved in regulating MT-dependent processes such as meiotic spindle alignment and chromosome congression at mitosis (Leader et al., 2002; Yasuda et al., 2004). Notably, both mDia1 and its interacting protein Pkd2 localize to mitotic spindles (Ishizaki et al., 2001; Kato et al., 2001; Rundle et al., 2004). In *Drosophila melanogaster*, the formin Cappuccino directly regulates Rho-dependent actin-MT cross talk during ooplasmic streaming and has an MT binding domain (Rosales-Nieves et al., 2006). In migrating fibroblasts, mDia1 stabilizes a subset of MTs downstream of lysophosphatidic acid (LPA)–induced Rho signaling (Palazzo et al., 2001; Wen et al., 2004; Goulimari et al., 2005; Eng et al., 2006). mDia may also contribute to MTOC orientation in fibroblasts and cytotoxic lymphocytes (Yamana et al., 2006; Gomez et al., 2007).

The current model for mDia-regulated stabilization of MTs suggests that LPA triggers a Rho/mDia-dependent pathway that also involves EB1, APC, GSK3β, and novel PKCs to generate a polarized array of stabilized MTs oriented toward the leading edge of cells in a wounded monolayer (Palazzo et al., 2001; Wen et al., 2004; Eng et al., 2006). The localization of these stabilized MTs is regulated by integrin signaling (Palazzo et al., 2004), and this is thought to contribute to cell polarity by directing vesicular trafficking and/or actin regulators to the leading edge (Lin et al., 2002). Rho/mDia-stabilized MTs are characterized by elevated levels of posttranslationally detyrosinated α-tubulin, which arises after stabilization through the removal of the C-terminal tyrosine residue (Gundersen et al., 1984, 1987). Detyrosination exposes a glutamate residue at the C terminus of the α-tubulin and, hence, stable MTs that contain elevated detyrosinated α-tubulin are referred to as Glu MTs, as opposed to more dynamic MTs, which contain tyrosinated α-tubulin and are referred to as Tyr MTs (Gundersen et al., 1984, 1987).

Analyses of MT plus-end turnover in cells have shown that the stabilization induced by LPA/Rho-mDia signaling is achieved by capping of MT plus ends, which makes them refractory to tubulin subunit exchange (Infante et al., 2000; Palazzo et al., 2001). The biochemical mechanisms of MT stabilization by Rho/mDia proteins are still poorly understood and it is unclear which proteins in the pathway are directly involved in stabilizing this class of MTs. To date, there is no evidence to support a role for formins in directly modulating the dynamics of the MT cytoskeleton, and it remains possible that MT stabilization is a secondary consequence of mDia-mediated assembly and stabilization of actin filaments. In this paper, we show that actin nucleation and MT stabilization by mDia2 are two separate cellular functions of this formin and, further, that the formation of a stable mDia2 dimer is not necessary for MT stabilization. We also demonstrate that purified mDia2 directly stabilizes MTs by inhibiting both polymerization and depolymerization rates and that this activity maps to the FH2 domain.

Results

I704A and K853A FH1FH2mDia2 mutants are defective in actin assembly in vitro and in vivo

Alanine substitutions of Ile 1431 and Lys 1601 completely abolish the actin-nucleating activity of the FH2 domain in the yeast formin Bni1p (Xu et al., 2004) and, at least in the case of the corresponding I704A mutation, in mammalian mDia2 (Harris et al., 2006). These substitutions also eliminate the ability of the FH2 domain to protect barbed ends from heterodimeric capping protein (Xu et al., 2004; Harris et al., 2006). We introduced the analogous mutations (I704A and K853A) in a constitutively active fragment of mDia2 that consists of both the FH1 and 2 domains and lacks the regulatory GBD and DAD domains (Fig. 1 A). We prepared the mutants in this fragment of mDia2 for three reasons: it is the minimal fragment of the protein that is fully active for MT stabilization in vivo (Wen et al., 2004); it is expected to retain its actin nucleation activity because it has intact FH1 and 2 domains; and it does not dimerize with mDia1 (Copeland et al., 2004).

We first prepared recombinant His-tagged proteins and tested them for actin assembly using a kinetic assay using pyrene-labeled actin (Fig. 1 B; Li and Higgs, 2003, 2005; Harris et al., 2006). Both mutants were reduced in stimulating actin assembly compared with their wild-type counterpart, with a >1,000-fold reduction in activity for the I704A mutant and 60–70-fold reduced activity for the K853A mutant. Thus, although the K853A mutation is intermediate in effect, the I704A is virtually dead for actin assembly.

To test whether the actin polymerization defect in vitro correlated with a loss of activity in vivo, we introduced wild-type and mutant forms of FH1FH2mDia2 into serum-starved NIH3T3 cells, which have low levels of assembled actin. We injected the proteins at the minimal concentration at which the wild-type fragment induced actin fibers as assessed by phalloidin staining. Under these conditions both mutants failed to induce actin fibers (Fig. 1, C and D). No dominant-negative effects of the mutant constructs were observed in cells that had been stimulated with LPA to induce stress fibers (unpublished data).

We used total internal reflection fluorescence (TIRF) microscopy to examine the directional movement of mDia2 puncta, which are thought to reflect actin filament growth (Higashida et al., 2004). Consistent with the inability of the mutants to induce actin filaments, we observed fast directional movement of EGFP-FH1FH2mDia2 puncta only with the wild-type construct, as we could not trace linear tracks for most of the EGFP puncta in cells with either of the mDia2 mutants (Fig. 1 E). As previously observed for an analogous mDia1 fragment (Higashida et al., 2004), wild-type EGFP-FH1FH2mDia2 puncta typically moved toward the cell periphery and accumulated at the tips of filopodia-like protrusions (Video 1, available at http://www.jcb.org/cgi/content/full/jcb.200709029/DC1). We confirmed that this movement was dependent on intact actin filaments, but not MTs, because it was blocked by latrunculin A and not by nocodazole (unpublished data). The velocity of

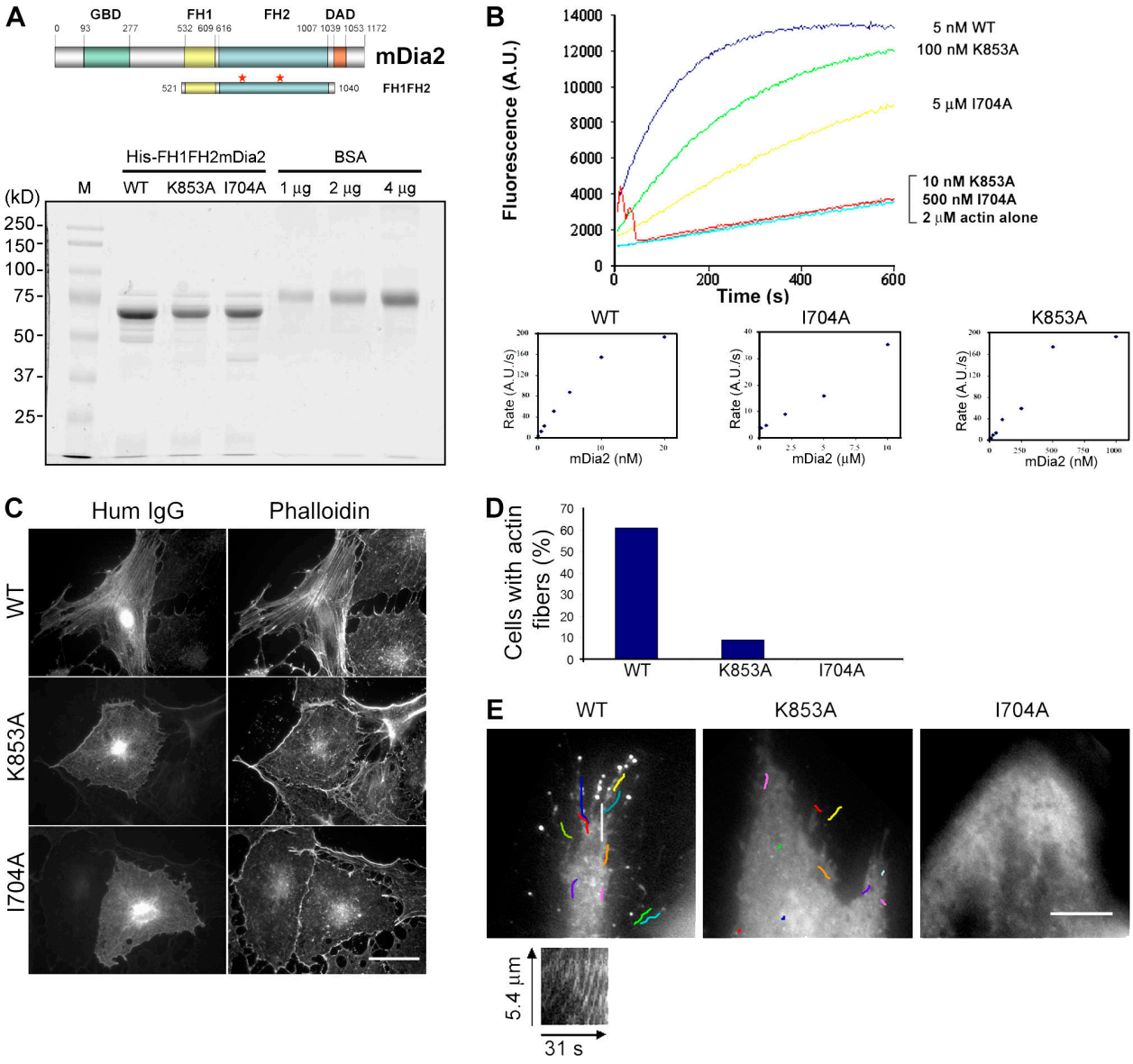

Figure 1. **K853A and I704A FH1FH2mDia2 point mutants are defective in actin polymerization.** (A) K853A and I704A point mutations (top, red stars) were introduced into a constitutively active fragment of mDia2 that includes the FH1 and 2 domains but lacks the GBD and DAD domains. HIS-tagged versions of the mutant (K853A and I704A) and wild-type (WT) proteins were expressed in *Escherichia coli*, affinity purified, and run on 10% SDS-PAGE followed by Coomassie staining. M, protein markers. (B) Pyrene-labeled monomeric actin was assembled in the presence of the indicated concentrations of wild-type and mutant His-FH1FH2mDia2. The panels below the graph show the rates of actin assembly at 50% polymerization in the presence of different concentrations of wild-type and mutant mDia2. Fluorescence is expressed in arbitrary units (A.U.), and all reactions were performed under identical conditions. (C) Rhodamine-conjugated phalloidin staining of serum-starved NIH3T3 cells microinjected with 8 µM of wild-type, I704A, or K853A His-FH1FH2mDia2 and human IgG as a marker. (D) Quantification of the percentage of cells injected with the indicated constructs of His-FH1FH2mDia2 that exhibit actin fibers ($n > 40$ cells). (E) TIRF microscopy of EGFP-FH1FH2mDia2 puncta in NIH3T3 cells. Shown is a single frame from movies taken of cells expressing wild-type or actin mutant EGFP-FH1FH2mDia2. Each color line indicates the track of a single EGFP punctum that could be followed for more than three frames. A kymograph of a selected region (white line) from the movie taken with a wild-type–expressing cell is shown below. Bars: (C) 10 µm; (E) 5µm.

wild-type EGFP-FH1FH2mDia2 puncta was 0.31 ± 0.16 µm/s, an order of magnitude faster than the flow rate of the actin network yet slower than the velocity estimated for GFP-FH1FH2mDia1 puncta (Higashida et al., 2004). Conversely, the K853A mutant generally traveled over shorter distances with very limited localization to filopodia tips, whereas the I704A mutant exhibited no clear directional movement with no accumulation at the cell periphery (Videos 2 and 3). We conclude that both mDia2 mutants do not associate processively with the barbed ends of growing actin filaments in vivo.

I704A and K853A FH1FH2mDia2 mutants induce stable Glu MTs and bind to APC and EB1

To test whether the actin-deficient FH1FH2mDia2 mutants were able to induce stable Glu MTs, we microinjected them into serum-starved NIH3T3 cells, which contain low levels of stable Glu MTs. Both EGFP-tagged mutants generated stable MTs, although the I704A mutant was reduced ~20% compared with the wild type (Fig. 2, A and B). Similar results were observed if His- or GST-tagged proteins were microinjected instead of expressing

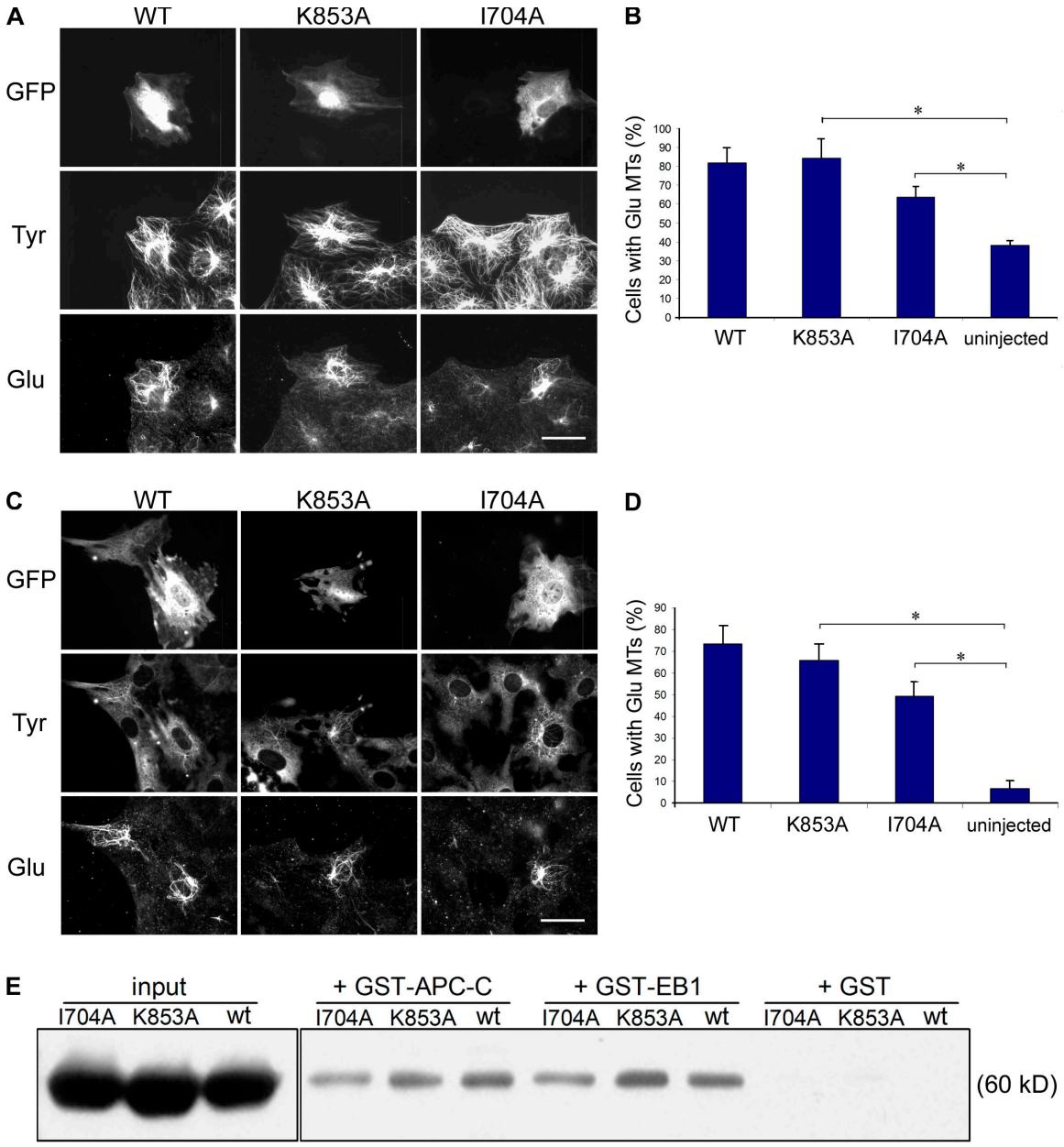

Figure 2. **K853A and I704A FH1FH2mDia2 induce stable Glu MTs.** (A) Glu and Tyr tubulin immunostaining of serum-starved NIH3T3 cells expressing indicated wild-type (WT) or actin mutant (I704A and K853A) EGFP-FH1FH2mDia2 constructs. (B) Quantification of cells injected with indicated constructs that exhibited stable Glu MTs (Glu). Data are mean ± SD from three independent experiments ($n > 50$ cells). Asterisks indicate $P < 0.001$, calculated by χ^2 test (one degree of freedom). (C) Glu and Tyr tubulin immunostaining of serum-starved NIH3T3 cells expressing indicated constructs and then treated with 2 μM nocodazole for 30 min. (D) Quantification of cells that exhibited stable Glu MTs after injection of indicated constructs and nocodazole treatment as in C. Data are mean ± SD from three independent experiments ($n > 50$ cells). Asterisks indicate $P < 0.001$, calculated by χ^2 test (one degree of freedom). (E) Western blot analysis of pulldown experiments using GST-EB1, GST-APC-C, or GST alone incubated with the indicated His-FH1FH2mDia2 proteins. Bound proteins were eluted and resolved by SDS-PAGE and mDia2 proteins were detected by mouse RGS-His antibody. Bars, 10 μm.

EGFP-tagged cDNAs (unpublished data). The Glu MTs induced by all the mDia2 constructs were resistant to 30-min incubation with 2 μM nocodazole, a treatment that depolymerizes dynamic MTs (Fig. 2, C and D). With the I704A mutant, the induced Glu MTs were frequently (~50% of cells) concentrated in a perinuclear area rather than extended to the cell periphery as observed in cells expressing the wild-type or K853A mutant. The I704A mutant was the most impaired in nucleating actin and in processive movements (Fig. 1, D and E), suggesting that these activities may still be required for producing or maintaining stable Glu MTs in the cell periphery. Alternatively, this defect could be caused by the inability of the I704A mutant to bind to either EB1 or APC, two necessary partners for mDia in stabilizing MTs downstream of Rho signaling. To test whether the mutants still bound to EB1 and APC, in vitro pulldown assays were performed with purified proteins (Fig. 2 E). Both mutants bound to EB1 or APC to a similar extent as with wild-type mDia2, suggesting a role for the retention of these interactions in the induction of stable Glu MTs and that the lack of extended Glu MTs in cells expressing the I704A mutant is presumably caused by another activity.

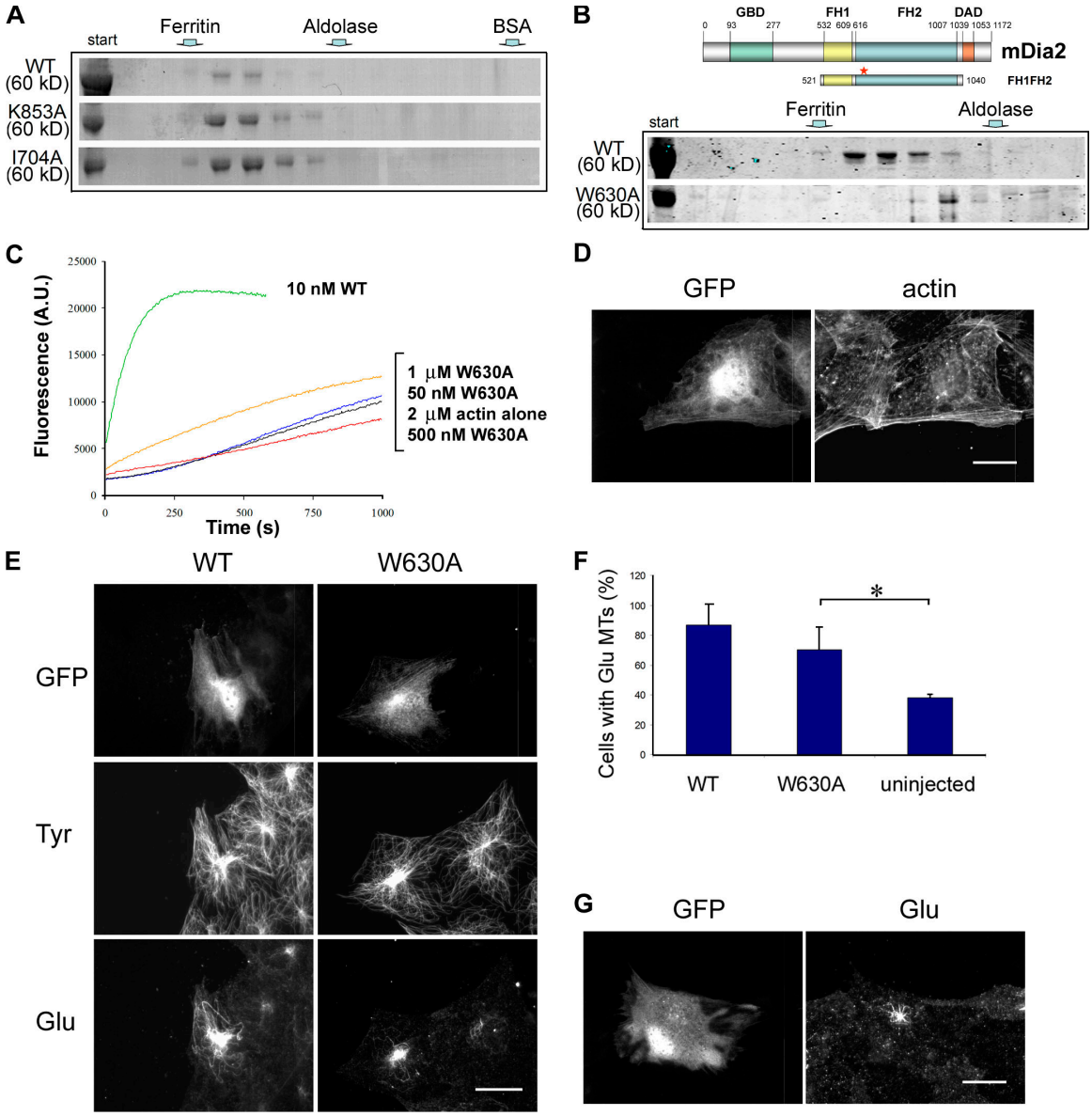

Figure 3. **The dimerization mutant W630A FH1FH2mDia2 induces stable Glu MTs.** (A) Elution profiles of the indicated His-FH1FH2mDia2 proteins from analytical Superdex 200 gel filtration. An aliquot of each fraction was analyzed by Western blotting using an anti-His antibody. The arrows indicate elution volumes of standards run under the same conditions. (B) Diagram of W630A His-FH1FH2mDia predicted to be a dimerization mutant (red star indicates the position of the mutation) and comparison of elution profiles of W630A and WT His-FH1FH2mDia2 proteins from analytical Superdex gel filtration analyzed by Western blotting as in A. (C) Pyrene-actin assembly assays using His-tagged wild type (WT) and increasing concentrations of W630A FH1FH2mDia2 (W630A). Fluorescence is expressed in arbitrary units (A.U.) and all reactions were performed under identical conditions. (D) Actin immunostaining of serum-starved NIH3T3 cells expressing microinjected EGFP-tagged W630A FH1FH2mDia2. (E) Glu and Tyr tubulin immunostaining of serum-starved NIH3T3 cells expressing microinjected EGFP-tagged wild-type or W630A FH1FH2mDia2. (F) Quantification of cells that exhibited stable Glu MTs after expression of indicated EGFP-tagged constructs. Data are mean ± SD from three independent experiments ($n > 70$ cells). Asterisk indicates $P < 0.001$, calculated by χ^2 test (one degree of freedom). (G) Glu tubulin immunostaining of nocodazole-resistant MTs in cells expressing EGFP-tagged W630A FH1FH2mDia2. Bars, 10 μm.

W630A FH1FH2 mDia2 dimerization mutant induces stable Glu MTs

A dimer appears to be the functional state of formin FH2 domains and is required to promote actin nucleation and elongation (Moseley et al., 2004; Shimada et al., 2004; Xu et al., 2004). We questioned whether a functional dimer is also necessary for the stabilization of the MT cytoskeleton and analyzed the dimerization properties of purified wild-type and mutant His-FH1FH2mDia2 proteins by analytical gel filtration (Fig. 3 A). The elution profile for all of these proteins was identical with a single peak at a volume consistent with the elution properties of analogous dimeric fragments of both mDia1 and mDia3 (Li and Higgs, 2003; Shimada et al., 2004).

We next tested whether a dimerization mutant, based on the crystal structure of the Bni1p FH2 domain, was capable of inducing stable Glu MTs in cells. We substituted Trp 630 with an Ala, as this residue localizes at the dimerization interface of Bni1 (Xu et al., 2004). Trp 630 is also among the most conserved amino acids in the FH2 domain (Moseley et al., 2004; Xu et al., 2004). Gel filtration analyses of the W630A FH1FH2mDia2

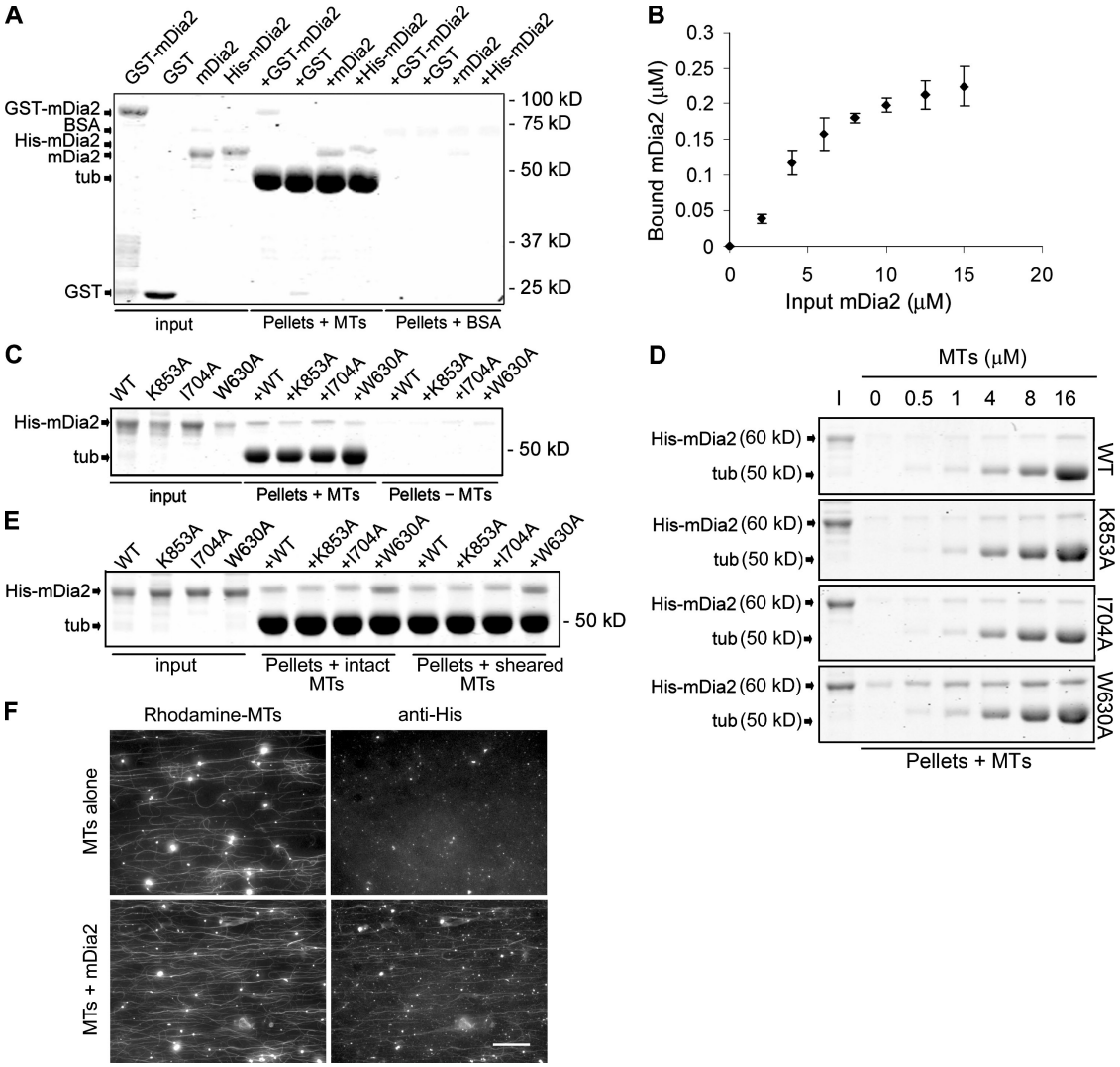

Figure 4. **FH1FH2mDia2 binds directly to MTs.** (A) SDS gel analysis of the cosedimentation of His- (His-mDia2), GST- (GST-mDia2), or untagged (mDia2) FH1FH2mDia2 or GST alone (GST) with taxol-assembled MTs or BSA. Matching input and pellet fractions were resuspended in SDS loading buffer and run on 10% SDS-PAGE followed by Coomassie staining. tub, tubulin. (B) Concentration dependence of FH1FH2mDia2 binding to taxol stabilized MTs (1.5 μM tubulin). Error bars show SEM of three independent experiments. (C) SDS gel analysis of MT cosedimentation assay, as described in A, with His-tagged versions of wild-type (WT) and mutant (K853A, I704A, and W630A) FH1FH2mDia2. (D) Concentration dependence of wild-type and mutant His-FH1FH2mDia2 binding to MTs. Input material (I) and MT (or BSA) pellets material are shown. (E) MT cosedimentation analyses of wild-type and mutant His-FH1FH2mDia2 with intact and sheared MTs. (F) Immunostaining of His-FH1FH2mDia2 on immobilized MTs as described in Materials and methods. Bar, 10 μm.

protein showed that it eluted as a major peak at a volume suggesting that it behaves as a monomer rather than a dimer (Fig. 3 B). We conclude that the W630A mutation generates a protein that is impaired in forming a stable dimer.

Because dimerization is a necessary requirement for processive actin filament association, we tested the ability of W630A FH1FH2mDia2 to promote F-actin assembly in vitro and in vivo. Pyrene-labeled actin polymerization assays showed that the W630A mutant was >250 times less active than the wild type in nucleating actin (Fig. 3 C). Actin staining of serum-starved cells microinjected with W630A EGFP-FH1FH2mDia2 showed no induction of actin fibers as was observed with the wild type (Fig. 3 D and Fig. 1 C). Moreover, virtually no directional movement of bright GFP particles was visualized in cells expressing this mutant mDia2 and no accumulation in filopodia protrusions was observed (Video 4, available at http://www.jcb.org/cgi/content/full/jcb.200709029/DC1). We conclude that the W630A mutant lost its ability to polymerize actin in vitro and in vivo.

When we tested the same construct for induction of stable Glu MTs, we observed that cells expressing W630A EGFP-FH1FH2mDia2 displayed more stable MTs than uninjected neighboring cells, although at a frequency 20% lower than that of cells expressing the wild-type protein (Fig. 3, E and F). Most of the Glu MTs (~90%) induced by the W630A mutant displayed the "knotted" phenotype that was observed with the most severe actin binding mutant. The stability of these Glu MTs was confirmed by testing their resistance to nocodazole treatment (Fig. 3 G). These data show that a stable dimer is not necessary to generate stable Glu MTs by mDia. Combined with the data from the actin-deficient mutants, these results reinforce the conclusion that promotion of actin polymerization and induction of MT stability by mDia2 can be functionally segregated.

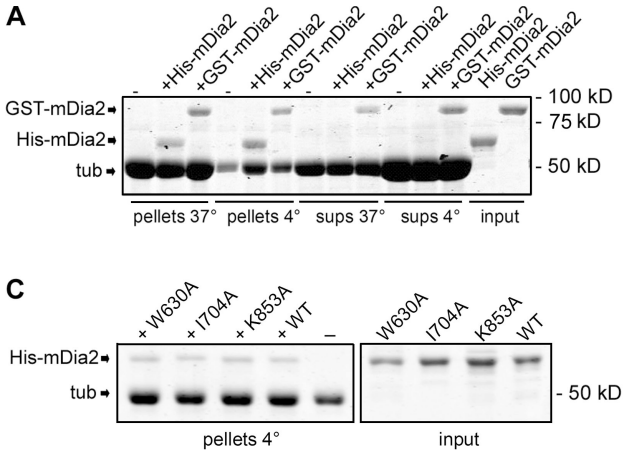

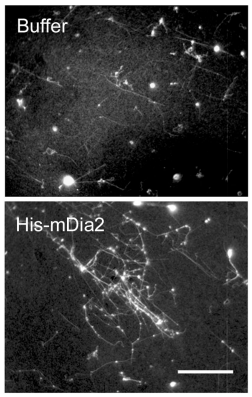

Figure 5. **FH1FH2mDia2 stabilizes MTs against cold-induced depolymerization.** (A) SDS gel analysis of the resistance of self-assembled MTs to cold-induced depolymerization after incubating with His- (His-mDia2) or GST- (GST-mDia2) tagged FH1FH2mDia2. After centrifugation, equivalent amounts of the pellets and supernatants were resolved by SDS-PAGE and visualized by Coomassie. (B) Immunostaining of MTs that survive cold-induced depolymerization in the presence of His-FH1FH2mDia2 (His-mDia2) or buffer alone. (C) SDS gel analysis of the resistance of self-assembled MTs to cold-induced depolymerization after incubating with wild-type and mutant His-FH1FH2mDia2. Pellets at 4°C and input material are shown. Panels shown are from a single gel. Bar, 10 µm.

mDia2 stabilizes MTs against depolymerization in vitro

In addition to our data, there is already some evidence suggesting there might be a direct role of mDia on MTs. Previous studies have shown that ΔGBDmDia2 localizes along the length of stabilized MTs (Palazzo et al., 2001). The related protein, mDia1, is also found at a low frequency at the ends of stable MTs in cells (Wen et al., 2004) and has been localized to the mitotic spindle (Kato et al., 2001). However, to date, there have been no studies to explore whether any member of the mDia family shows direct biochemical activity toward MTs. We tested whether mDia2 might exhibit direct MT binding and stabilizing activity and, if so, whether this activity was sufficient to generate capped MTs in vitro, a defining characteristic of Glu MTs in vivo.

We first looked at binding of purified recombinant mDia2 to purified MTs or tubulin dimers. We incubated purified His-, GST-, or untagged versions of FH1FH2mDia2 with taxol-assembled MTs or BSA, followed by high-speed centrifugation to separate the MT pellet from soluble unbound material. Both tagged and untagged mDia2 were substantially recovered in the pellet fraction only when MTs were present (Fig. 4 A). In contrast, we did not detect any binding of FH1FH2mDia2 with tubulin dimer alone by gel filtration, native gel electrophoresis, or Biocore analyses (unpublished data). Binding of FH1FH2mDia2 to MTs was saturable with an estimated stoichiometry at saturation of 1:4.7 (mDia2/tubulin) and an estimated K_D of 6.1 µM (Fig. 4 B). Similar binding to MTs was observed for the K853A, I704A, and W630A FH1FH2 mutants, although the W630A mutant appeared to bind with higher affinity (Fig. 4, C and D). Shearing MTs to increase the number of MT ends did not detectably affect binding of wild-type or mutant FH1FH2mDia2 to MTs (Fig. 4 E). Consistent with the stoichiometry and lack of evidence for preferential end binding, FH1FH2mDia2 was localized along the length of MTs by immunostaining (Fig. 4 F). These results show that FH1FH2mDia2 directly binds to MTs and appears to interact with the sides of the MT.

We next tested the effect of mDia2 on MT stability and incubated substoichiometric amounts of His- or GST-FH1FH2mDia2 proteins with purified tubulin during spontaneous assembly of MTs at 37°C, followed by a short incubation at 4°C to induce rapid MT depolymerization. SDS gel analyses of MT pellets showed that addition of His- or GST-tagged FH1FH2mDia2 did not increase the level of MTs pelleting at 37°C but did increase the level of MTs pelleting after cold treatment, which is consistent with a role for mDia2 in MT stabilization (Fig. 5 A). Similar cold stability of MTs was observed when FH1FH2mDia2 was added to preassembled MTs (unpublished data). The stabilizing effect of mDia2 on MTs was concentration dependent and independent of the presence of a tag on mDia2, as untagged FH1FH2mDia2 also stabilized MTs against cold treatment (Fig. S1, available at http://www.jcb.org/cgi/content/full/jcb.200709029/DC1). We confirmed by immunofluorescence microscopy that a substantial number of MTs resisted cold depolymerization when mDia2 was present (Fig. 5 B) and found that both the actin and dimerization mutants of mDia2 retained this activity (Fig. 5 C). We conclude that FH1FH2mDia2 is sufficient to directly stabilize MTs against cold-induced depolymerization.

Glu MTs in extracted cells are characteristically resistant to disassembly upon dilution (Infante et al., 2000). Thus, we tested whether wild-type and mutant versions of FH1FH2mDia2 fragments could stabilize MTs assembled from purified tubulin against dilution-induced depolymerization. Controls in which MTs were diluted into BSA, heat-denatured mDia2, or His-tagged GSK3β showed low levels of MTs remaining as assayed by immunofluorescence (Fig. 6 A). In contrast, dilution of MTs into wild-type, actin (I704A, K853A), or dimerization (W630A) mutants of FH1FH2mDia2 all reduced dilution-induced MT depolymerization, as indicated by the increased number and length of MTs remaining after dilution (Fig. 6 A). We also noticed that the MTs persisting in the samples incubated with mDia2 proteins consistently appeared thicker than in the control samples, suggesting that mDia2 may also bundle MTs. We confirmed that FH1FH2 mDia2 bundled MTs by low-speed sedimentation assays of MTs in the presence of wild-type FH1FH2mDia2 (Fig. S2, available at http://www.jcb.org/cgi/content/full/jcb.200709029/DC1).

We next used the MT dilution assay to map the MT-stabilizing activity in FH1FH2mDia2. Recombinant fragments of mDia2 lacking the FH1 and the N terminus of the FH2 (FH2ΔN), portions of the FH2 (FH1FH2ΔC), or both (FH2C) were tested for their ability to protect MTs from dilution-induced depolymerization (Fig. 6, A and B). Each of these fragments

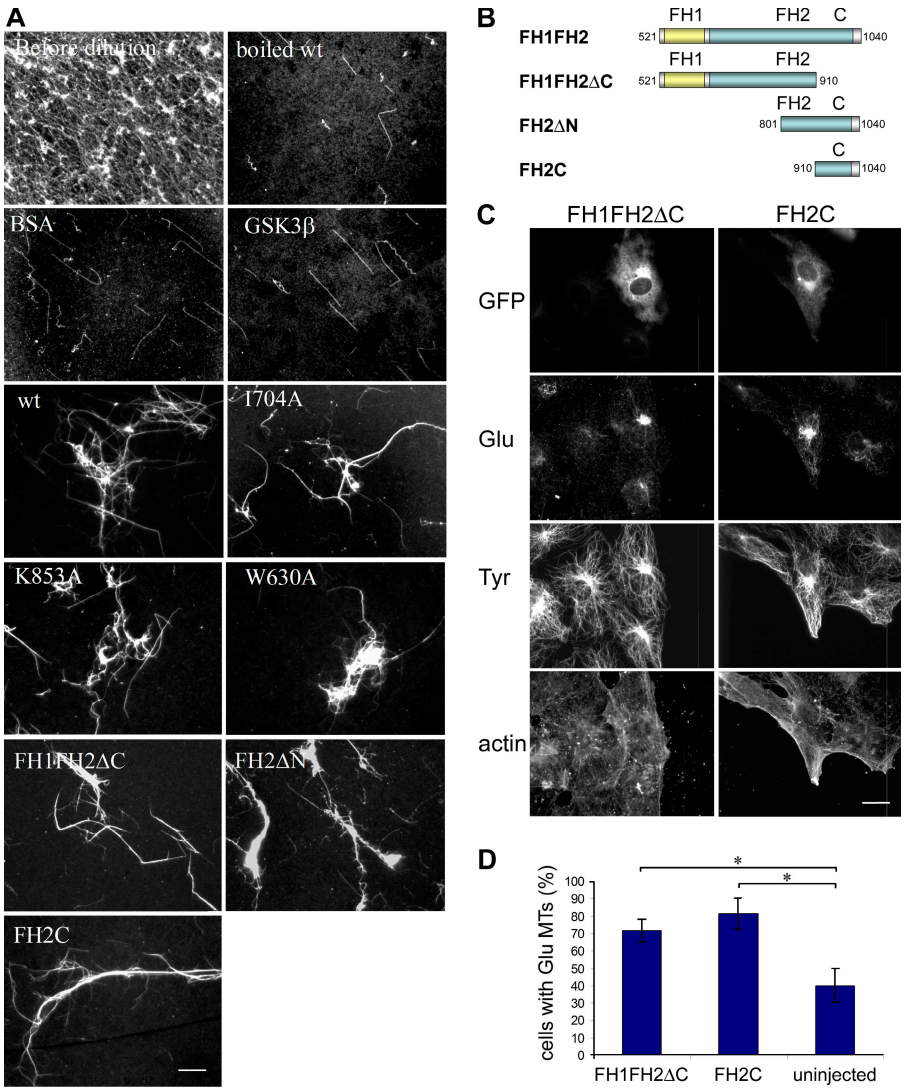

Figure 6. **FH1FH2mDia2 stabilizes MTs against dilution-induced disassembly and the activity maps to the FH2 domain.** (A) Immunostaining of MTs that survived dilution induced depolymerization upon incubation with the following indicated proteins (all proteins were His-tagged except BSA): GSK3β, glycogen synthase kinase 3β; WT, wild-type FH1FH2mDia2; I704A, K853A, and W630A, mutant FH1FH2mDia2; FH1FH2ΔC, FH2ΔN, and FH2C, fragments of FH1FH2mDia2 (see B). (B) Diagram of fragments of FH1FH2mDia2 used for MT stability tests in A. (C) Immunostaining of Glu and Tyr MTs and actin in wounded starved NIH3T3 fibroblasts expressing EGFP-FH1FH2ΔC or EGFP-FH2C-mDia2. (D) Quantification of cells expressing the indicated constructs that exhibited stable Glu MTs. Data are mean ± SD from three independent experiments ($n > 70$ cells). Asterisk indicates $P < 0.001$, calculated by χ^2 test (one degree of freedom). Bars, 10 μm.

stabilized MTs against dilution-induced depolymerization (Fig. 6 A). Collectively, these results suggest that at least two MT stabilization sites are present in FH1FH2mDia2: one encompasses residues 521–910 (FH1FH2ΔC) and the other residues 910–1040 (FH2C).

We next tested whether the FH1FH2ΔC and FH2C fragments induced stable MTs in serum-starved cells and found that both induced stable Glu MTs above background levels (Fig. 6, C and D). Interestingly, as previously noted for the mDia2 actin and dimerization mutants, these Glu MTs appeared knotted and clustered at a perinuclear region rather than extending to the cell periphery as observed for stable Glu MTs induced by LPA. To examine whether this knotted phenotype reflected a loss in actin nucleation activity, we tested these fragments for their ability to assemble F-actin. Neither deletion construct induced formation of actin filaments comparable to FH1FH2mDia2 levels in serum-starved cells (Fig. 6 C). The FH2C fragment also showed almost a 1000-fold lower activity than FH1FH2mDia2 in pyrene-actin assembly assays (Fig. S3, available at http://www.jcb.org/cgi/content/full/jcb.200709029/DC1). In addition, no linear trajectories of EGFP particles were observed when EGFP-tagged versions of these fragments were transfected into NIH3T3 cells and analyzed by TIRF microscopy (unpublished data). These results were not surprising, as an intact FH2 dimer is required for productive interactions of formins with actin (Moseley et al., 2004; Xu et al., 2004). The loss of actin assembly activity in these fragments of mDia2 that maintain MT stabilizing activities confirms a clear separation between mDia2 activities on actin and MTs.

mDia2 decreases tubulin dissociation rates in vitro

MT stabilization by the Rho–mDia pathway occurs by inhibition of tubulin loss and gain at MT ends (Palazzo et al., 2001). The stability assays employed in the experiments shown in Figs. 4, 5, and 6 do not reveal whether the MT stabilization activity of mDia2 is mediated by an inhibitory effect on tubulin dissociation/association rates, the frequency of transitions to rapid shortening phases (catastrophe), or both. To gain insight into the mechanism of MT stabilization by mDia2, we tested whether mDia2 affected individual parameters of MT assembly/disassembly by monitoring the behavior of individual MTs assembled from

purified axonemal fragments using video-enhanced differential interference contrast (DIC) microscopy. MTs assembled in the presence of His-FH1FH2mDia2 had significantly slower rates of assembly at both plus and minus ends compared with those of MTs assembled from purified tubulin alone (Table I). Although these effects were relatively modest (~25% inhibition of control rates for both plus and minus ends), these data demonstrate that mDia2 inhibits tubulin addition at MT ends. No significant difference was observed in the catastrophe frequencies (C_f) or rates of shortening (V_s) during MT assembly in the presence of mDia2. However, because catastrophes and shortening events are rare under MT assembly conditions, we also explored the effect of FH1FH2mDia2 on MTs under disassembly conditions, where shortening events are predominant and can be analyzed with higher statistical confidence. In these experiments, MTs were first assembled on axonemes and then the chamber was perfused with either buffer alone or His-FH1FH2mDia2 diluted in buffer to initiate MT depolymerization. As shown in Fig. 7 A, MTs diluted into His-FH1FH2mDia2 depolymerized more slowly than MTs diluted into buffer alone (Videos 5 and 6, available at http://www.jcb.org/cgi/content/full/jcb.200709029/DC1). Quantification of this effect showed that in His-FH1FH2mDia, both MT plus and minus ends shortened at ~60% of the rate of MTs diluted into buffer alone (Fig. 7 B). The decrease in shortening rate with His-FH1FH2mDia2 was concentration dependent and saturated at ~2 μM mDia2 (Fig. 7 C). Interestingly, when MTs were induced to depolymerize in the presence of His-FH1FH2mDia2, we occasionally observed individual MTs abruptly switching to a slower shortening rate that approached zero (Fig. 7 D). This time-dependent change in the shortening rate occurred only at plus ends. We quantified this behavior by counting shortening ends in which the rate slowed to 50% or less of the starting shortening rate for that MT and found that for 2 μM mDia2, 14.7% of plus ends shifted to a slower shortening rate compared with 0% for the buffer control. Collectively, these data demonstrate that His-FH1FH2mDia2 stabilizes MTs by inhibiting both the polymerization and depolymerization rates at MT ends and suggest that this activity may contribute to the induction of MT stability in vivo.

Table I. **Dynamics of MTs assembled with FH1FH2mDia2 or buffer alone**

	Plus ends	Minus ends
Buffer	V_e = 1.82 ± 0.54 (25)	V_e = 0.99 ± 0.23 (21)
	T_e = 0.95 ± 0.59 (25)	T_e = 0.96 ± 0.57 (21)
	V_s = 30.20 ± 7.90 (11)	V_s = 27.67 ± 11.76 (3)
	T_s = 0.21 ± 0.09 (11)	T_s = 0.17 ± 0.06 (3)
	C_f = 0.44 ± 0.13 (11)	C_f = 0.14 ± 0.08 (3)
mDia2	V_e = 1.42 ± 0.47 (30)**	V_e = 0.75 ± 0.45 (40)*
	T_e = 0.97 ± 0.62 (30)	T_e = 1 ± 0.58 (40)
	V_s = 35.57 ± 14.78 (8)	V_s = 28.73 ± 26.07 (6)
	T_s = 0.15 ± 0.07 (8)	T_s = 0.25 ± 0.22 (6)
	C_f = 0.27 ± 0.09 (8)	C_f = 0.14 ± 0.05 (6)

Dynamics obtained with axonemal fragments using 10 μM PC tubulin and 2 μM His-FH1FH2mDia2 (mDia2) or buffer alone. Values are mean ± SD with the number of MTs observed indicated in parentheses. V_e, elongation rate (μm/min); T_e, time spent in elongation (min); V_s, shortening rate (μm/min); T_s, time spent in shortening (min); C_f, catastrophe frequency (min^{-1}). *, $P < 0.05$; **, $P < 0.01$ (Student's *t* test).

Discussion

Formins have been extensively characterized for their ability to nucleate and elongate actin filaments (Goode and Eck, 2007). However, their regulation of the MT cytoskeleton, which has been documented both in dividing and migrating cells, is poorly understood. In NIH3T3 cells, mDia1 is both necessary and sufficient to stabilize a subset of MTs (Glu MTs) arranged in the direction of migration downstream from Rho signaling (Palazzo et al., 2001; Goulimari et al., 2005; Eng et al., 2006). mDia also participates in MT stabilization in embryonic endodermal cells and C6 glioma cells (Kodama et al., 2003; Yamana et al., 2006), and evidence exists that mDia associates with MTs and MT ends in vivo (Kato et al., 2001; Palazzo et al., 2001; Wen et al., 2004). However, given the potent and direct effects of mDia on actin assembly, it has remained unclear whether the MT effects might occur as a secondary consequence of mDia-induced actin assembly in cells. In this paper, we show that promotion of actin polymerization and induction of stable Glu MTs by mDia2 can be functionally separated, as two actin polymerization-defective mutants of mDia2 were capable of inducing stable Glu MTs in NIH3T3 cells (Figs. 1 and 2). We also demonstrate that a stable mDia2 dimer is not required to generate stable Glu MTs (Figs. 3 and 6). As the stable dimer is thought to be the functional state of formins during actin assembly (Copeland et al., 2004; Moseley et al., 2004; Xu et al., 2004), this finding reinforces the notion that processive barbed end actin assembly and induction of MT stability are functionally separable. Interestingly, the ablation of actin assembly or processive barbed end actin filament association by mDia2 mutants was consistently coupled to induction of stable Glu MTs that appeared knotted around the centrosome instead of being fully extended to the cell periphery (Figs. 2, 3, and 6). We have not analyzed the cause of this phenotype, but as cells that express mutant mDia2 showed normal cell morphology and had a normal distribution of Tyr MTs, it appears that the perinuclear localization of Glu MTs was not a result of cell contraction or global effects on MTs. Rather, this phenotype suggests that the ability of mDia2 to function on the actin cytoskeleton may still be required for proper distribution of stable MTs, specifically to orient stable MTs toward the leading edge. Perhaps mDia's ability to interact with dynamic actin filaments at this cellular site creates a localized pool of mDia that can also interact with nearby MTs. Interestingly, integrin engagement and clustering into focal adhesions, which is partly dependent on mDia (Riveline et al., 2001; Yamana et al., 2006), is also necessary for formation of stable Glu MTs oriented toward the leading edge (Palazzo et al., 2004).

The finding that actin remodeling by mDia2 was not required for stabilizing MTs in cells prompted us to test whether formins could affect MT stability directly. Indeed, we observed that an FH1FH2 fragment of mDia2 stabilized MTs assembled from purified tubulin against depolymerization induced by either cold or tubulin dilution (Figs. 4, 6, and 7). As induction of

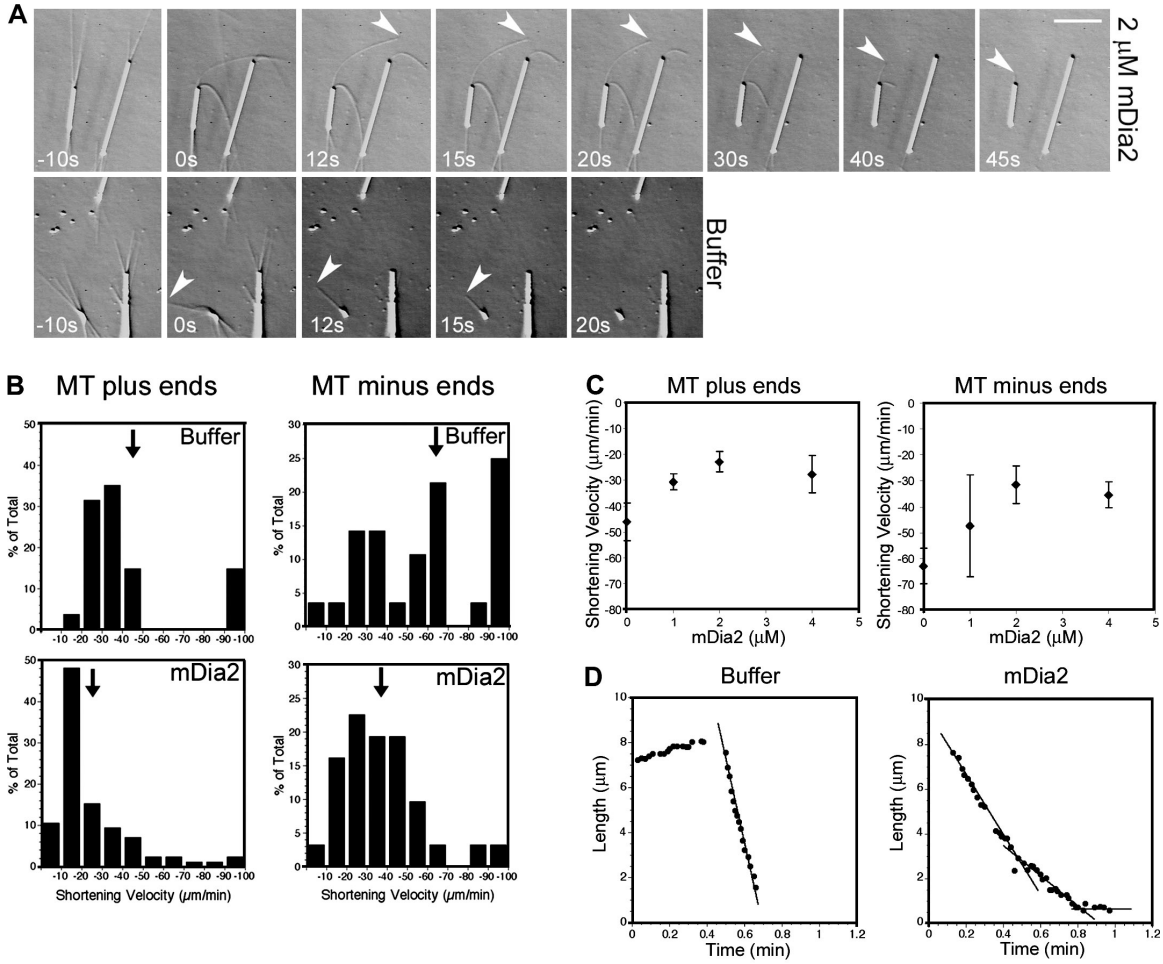

Figure 7. **FH1FH2mDia2 stabilizes MTs by decreasing rates of MT disassembly.** (A–D) Disassembly assays of MTs elongating from axonemal fragments and induced to disassemble by dilution in the presence or absence of the indicated concentrations of His-FH1FH2mDia2 or buffer alone. The rate of MT shortening was monitored by real-time video DIC microscopy. (A) A series of micrographs taken from a real-time video recording of MTs undergoing shortening. Arrowheads point to MT ends shortening in the presence of 2 μM His-FH1FH2mDia2 (mDia2) or buffer alone. Time is shown in seconds. (B) Histogram of the frequency of final shortening velocities of MT plus and minus ends after dilution into 2 μM His-FH1FH2Dia2 or buffer alone. Arrows indicate means for each condition. Data are normalized percentages of total MTs (to account for differences in sample size; $n \geq 53$ ends for each condition). Velocities >90 μm/min are pooled in the last bin. (C) Graphs showing the dependence of shortening velocity of MT plus and minus ends on concentration of His-FH1FH2mDia2 (mDia2). Data are mean ± SE of shortening velocities (n ranges from 3 to 27 for each data point). (D) Plots of life histories of representative MT plus ends induced to disassemble by dilution into buffer alone or into buffer with 2 μM His-FH1FH2mDia2. Bar, 5 μm.

MT stability by mDia2 was also observed in assays with perfusion chambers where the concentration of free tubulin is essentially negligible after dilution, we suspected that stabilization would be mediated by inhibition of polymer dynamics rather than by stimulation of dimer assembly. Consistent with this idea, we found no evidence for mDia2 interacting with tubulin dimers and observed a small, but significant, decrease in the rate of MT polymerization when mDia2 was incubated with tubulin during assembly (Table I). An even larger effect of mDia2 was observed on rates of MT shrinkage and, in a small percentage of cases, this effect led to MTs that exhibited shrinkage rates near zero. The ability of mDia2 to strongly slow MT shrinkage rates is presumably related to mDia's role in generating stable MTs in vivo that do not shrink for extended intervals and behave as if they are capped (Cook et al., 1998; Infante et al., 2000; Palazzo et al., 2001). In this respect, mDia2's effect on MTs is distinct from traditional MAPs, which increase MT assembly rates without significantly interfering with MT shrinkage rates under similar experimental conditions (Drechsel et al., 1992; Pryer et al., 1992; Vasquez et al., 1994).

Although mDia2's ability to stabilize MTs in vitro is consistent with its activity in generating stable MTs in vivo, the in vitro experiments with axonemes showed that mDia2 did not completely block MTs from growing or shrinking, respectively, as is observed for Rho/mDia-stabilized MTs in vivo. One possibility is that full-length mDia2 has significantly greater activity toward MTs than the FH1FH2 fragment we used in the in vitro experiments. It also seems likely that the capping of MTs observed in vivo requires additional cellular factors that function with mDia. Indeed, APC and EB1, two MT binding proteins themselves, interact with mDia and have been implicated in generating stable MTs induced by LPA (Wen et al., 2004). Also, mDia regulation of GSK3β through novel PKCs has been recently shown to promote MT stabilization in migrating fibroblasts (Eng et al., 2006). It is possible that these factors, and maybe others yet to be discovered, contribute to cap MTs

in vivo. This may be accomplished by the formation of a multiprotein complex at MT plus ends in which all the players contribute to the stabilization activity. Because we have localized FH1FH2mDia2 predominantly to the sides of MTs (Fig. 4, E and F), it will be important to determine whether these additional factors restrict the activity of mDia2 toward MT ends or whether side binding to MTs by mDia2 contributes to the recruitment of other stabilizing factors to the plus end.

We attempted to narrow down the MT stabilization activity on mDia2 but found that there are at least two domains within the FHIFH2 fragment. We could not purify a His-tagged FH1 fragment of mDia2, yet no MT binding was detected for in vitro–translated FH1 fragment (unpublished data). These data suggest that the FH2 fragment contains at least two MT stabilization sites: one encompassing residues 616–910 and the other encompassing residues 910–1040. Each site is sufficient to induce MT stability in vitro and in vivo. The presence of two separate MT binding sites is also consistent with stabilization induced by a dimerization-defective W603A mutant of mDia2 and may explain the apparent bundling of MTs observed in the dilution assays (Figs. 3, 6, and S2). Bundling of MTs with actin filaments has previously been observed for Cappuccino, a related formin in *D. melanogaster* (Rosales-Nieves et al., 2006). Although bundling of MTs with themselves or with actin filaments could contribute to MT stability, we note that it cannot explain all of mDia2's stabilizing activity toward MTs because mDia2 also enhanced stability of individual MTs in the axonemal assays.

Our results show that the MT stabilization domain of mDia2 maps within the same region that is involved in actin polymerization (FH2 core domain). This finding raises the possibility that there is competition between the two cytoskeletal systems for mDia2. Importantly, the activity of mDia2 for actin is in the nanomolar range, whereas that for MTs is in the micromolar range. A simple competition model would predict that if actin and MTs exhibit mutually exclusive for binding to mDia, then redistribution of the formin to the MT cytoskeleton can only occur if the affinity for MTs is significantly increased. Potentially, this may be mediated by any of several regulatory proteins already implicated in stable Glu MT formation downstream of LPA signaling, including the MT TIP proteins APC and EB1 (Wen et al., 2004) and the kinases novel PKC and GSK3β (Eng et al., 2006). Selective activation of these mDia partners could localize mDia to MTs by preferential association of the complexes to MTs or by blocking high-affinity actin binding sites on the formin itself.

FH1FH2mDia2 fragments can stabilize MTs directly by inhibiting MT dynamics (Figs. 4, 6, and 7) and the stabilization activity maps to the FH2 domain of mDia2, the most conserved region among DRFs. These observations indicate that induction of MT stability is likely to be a shared feature of many DRFs. To date, only mDia1 has been shown to be necessary for stable MT formation in migrating cells. It will be important to test whether other DRFs can stabilize MTs directly and whether this activity is required in other cellular processes in which DRFs have already been implicated, such as cell adhesion, mitosis, or organelle trafficking.

Materials and methods

Chemicals

All chemicals were obtained from Sigma-Aldrich unless otherwise noted.

Cell culture, microinjection, and transfection

NIH3T3 cells were grown in DME and 10% calf serum as previously described (Cook et al., 1998; Kreitzer et al., 1999; Palazzo et al., 2001). For microinjection, confluent NIH3T3 cells grown on acid-washed coverslips were serum starved for 48 h in DME plus 10 mM Hepes, pH.7.4, and wounded for 30 min before being microinjected as previously described (Cook et al., 1998; Kreitzer et al., 1999; Palazzo et al., 2001). DNA plasmids in HKCL buffer (10 mM Hepes, pH.7.4, and 140 mM KCl) at 50–200 μg/ml were microinjected into nuclei and allowed to express for 2 h. Purified proteins were microinjected into the cytoplasm in HKCL buffer at 2 mg/ml, unless otherwise indicated, and incubated for 1 h and 30 min before fixation. In the experiments in which His-FH1FH2mDia2 proteins were used, 1 mg/ml of the fusion protein was coinjected with 5 mg/ml of the injection marker human IgG. NIH3T3 cells were transfected in growth medium (DME with 10% calf serum) with Lipofectamine Plus (Invitrogen), according to the manufacturer's specifications, and allowed to express for an additional 18–24 h.

Plasmid construction

pGST−APC-C (aa 2167−2843) and GST-FH1FH2mDia2 (aa 521–1040) were gifts from R. Baer (Columbia University, New York, NY) and A. Alberts (Van Andel Institute, Grand Rapids, MI), respectively. pGST-EB1 and pHis-FH1FH2mDia2 were constructed as described previously (Wen et al., 2004). pEGFP-FH1FH2mDia2 was prepared by subcloning 521–1040-mDia2 from pEFm-EGFP (Wen et al., 2004) into pEGFP-C1 (Clontech Laboratories, Inc.). K853A, I704A, and W630A mDia2 point mutants were generated on pGST-FH1FH2mDia2 using the QuikChange Site-Directed Mutagenesis kit (Stratagene) according to the manufacturer's protocol and using the following synthetic sense oligonucleotide primers: 5′-ttgctcagaaccttcagccttcctgagctccttccg-3′ (I704A); 5′-ctctgtaaactgaaggatacagcatctgcagatcagaaaaccaca-3′ (K853A); and 5′-gaaatcagcatgagaagattgaatgcgttaaagatcggaccaaatgaaat-3′ (W630A). All mutations were subcloned into pEGFP-C1 and pQ30E by cutting the inserts with BamH1 and Xho1 and the vectors with BamH1–Xho1 or BamH1–Sal1, respectively. His-FH1FH2mDia2 deletion constructs were all generated by PCR amplification of pQ30E-FH1FH2mDia2 using KOD HiFi polymerase (EMD) and the following sense oligonucleotide primers: 5′-gcggatccgcagagttacaagctt-3′ (His-FH1FH2ΔC); 5′-gcggatccgctgtcagtactg-3′ (His-FH2ΔN); and 5′-gcggatccgagaagaatttggaa-3′ (His-FH2C). 5′-gcggtaccctgttgaagctgccttc-3′ (His-FH1FH2ΔC) and 5′-gcggtacccactcctgtctcatctc-3′ (His-FH2ΔN and His-FH2C) were chosen as the antisense oligonucleotide primers. pEGFP-FH1FH2ΔC and pEGFP-FH2C were constructed by subcloning the inserts from pQ30E into pEGFP-C1 using BamH1–Kpn1 and Bgl2–Kpn1 to cut inserts and vector, respectively. All constructs were verified by sequencing, and DNA was purified with midiprep kits (QIAGEN).

Protein purification and GST pulldown assays

GST-tagged proteins (GST-APC-C aa 2167−2843, GST-EB1, and wild-type GST-FH1FH2mDia2) and wild-type and mutant His-FH1FH2mDia2 were expressed in *E. coli* BL-21 or XL-1 blue cells and affinity purified on agarose-coupled glutathione (GE Healthcare) or nickel resin (Clontech Laboratories, Inc.), respectively, according to the manufacturer's recommended protocols. Untagged FH1FH2mDia2 was obtained by thrombin-mediated cleavage of the GST from the GST fusion protein according to the manufacturer's protocol. Purified proteins were resuspended in HKCL buffer plus 1 mM DTT using Sephadex G-25 PD-10 desalting columns (GE Healthcare). Direct binding was performed by incubating 0.3 μM His-FH1FH2mDia2 with 0.3 μM GST−EB1 or GST−APC-C in modified RIPA buffer (PBS, 1% Nonidet-P40, 1% sodium deoxycholate, 0.1% SDS, and protease inhibitor cocktail) for 18 h at 18°C as previously described (Wen et al., 2004). Bound proteins were analyzed by Western blotting with mouse RGS-His antibody (1:10,000).

Gel filtration assays

Affinity purified His-FH1FH2mDia2 proteins were analyzed by size exclusion chromatography using a Superdex 200 HR 10/30 column (GE Healthcare) and a Controller LCC-501 Plus FPLC system (GE Healthcare). The column was preequilibrated and run in HKCL buffer plus 1 mM DTT. The elution was monitored by absorbance at 280 nm and verified by SDS-PAGE of column fractions followed by Western blotting using mouse RGS-His

antibody (1:10,000). The size standards used were ferritin (440 kD), aldolase (158 kD), and BSA (67 kD).

Actin assembly kinetics

Actin filament assembly assays were performed in 60-µl reactions as previously described (Moseley et al., 2006). In brief, gel-filtered monomeric actin (final concentration 2 µM, 5% pyrene labeled) was converted to Mg-ATP-actin, mixed with the indicated proteins in HKCL buffer or HKCL buffer alone, and then added immediately to 3 µl of 20× initiation mix (40 mM $MgCl_2$, 10 mM ATP, and 1 M KCl). Pyrene fluorescence was monitored at excitation 365 nm and emission 407 nm in a fluorescence spectrophotometer (Photon Technology International) held at the constant temperature of 25°C. The rates of actin assembly were determined from the slopes of the assembly curves at 50% polymerization.

Epifluorescence and TIRF microscopy

Cells were either fixed in −20°C methanol for 10 min and rehydrated in TBS or fixed in 4% PFA in PBS for 10 min followed by permeabilization with 0.5% Triton X-100 in PBS for 5 min. Glu MTs were detected with a polyclonal rabbit antibody SG that specifically recognizes detyrosinated (Glu) tubulin (Gundersen et al., 1984; 1:400), and tyrosinated (Tyr) MTs were detected with the rat mAb YL1/2 (1:10; European Collection of Animal Cell Cultures). Rhodamine-phalloidin (1:500; Invitrogen) or mouse mAb to actin (C4D6; 1:200) were used to detect the actin cytoskeleton as specified. Secondary antibodies were obtained from Jackson ImmunoResearch Laboratories and were absorbed to minimize cross reaction with other species. Immunostained samples were observed with a microscope (Optiphot; Nikon) using a 60× plan apo objective (1.4 NA) and filter cubes optimized for coumarin, fluorescein/GFP, rhodamine, and Cy5 fluorescence (Nikon). Images were captured with a cooled charge-coupled device camera (MicroMax; KAF 1400 chip; Kodak) using Metamorph software (MDS Analytical Technologies).

For live-cell imaging experiments by TIRF microscopy, preparations were observed using a 60× plan apo objective (1.45 NA) on a microscope (TE2000-U; Nikon) equipped with a TIRF illuminator and fiber optic–coupled laser illumination. TIRF illumination was obtained with a separate laser line (Ar ion; 488 nm) using a filter cube optimized for fluorescein/GFP fluorescence (Chroma Technology Corp.). Images were captured with a cooled charge-coupled device camera (Orca ERI; Hamamatsu) using Metamorph software. For live-cell imaging of GFP-fusion mDia2 constructs by TIRF, cells were transfected 24 h before microscopy and images were acquired every 200 ms in GFP recording medium (Ho et al., 1998) plus 1 mM sodium pyruvate and 1% calf serum at 37°C. Kymographs were generated using Metamorph software from image stacks (47 frames) of the selected regions from each transfected cell as indicated. To measure the speed of each particle, a line region was drawn onto the kymograph and width and length logged into Excel (Microsoft). The mean speed was calculated for at least 10 particles. All images for figures were processed with Photoshop (Adobe).

MT binding assays

PC or DEAE tubulin at 25 µM (purified as described in Mikhailov and Gundersen [1995] and Tian et al. [1997]) was polymerized in PEMG buffer (100 mM Pipes-KOH, pH 6.9, 1 mM EGTA, 2 mM $MgCl_2$, and 1 mM GTP) with 10 µM Taxol at 37°C for 1 h. 12.5 µM of polymerized MTs was incubated with 1 µM of purified mDia2 fragments or BSA for 10 min at 30°C. MT pellets were recovered by centrifugation at 100,000 *g* for 10 min at 37°C, and matching aliquots of input and MT pellets were loaded onto a 10% SDS-PAGE. Proteins were detected by Coomassie staining. Saturation binding was measured using a range of concentrations of His-FH1FH2mDia2 (0–15 µM) and a fixed amount of MTs (1.5 or 3 µM). MT-bound mDia2 was estimated by Coomassie staining by comparison with a protein standard of known concentration run on the same gel. The fraction of mDia2 sedimenting in the absence of MTs was subtracted from each data point. K_D and stoichiometry of binding at theoretical saturation were calculated as best fit values using Prism 4 (GraphPad) assuming one site of binding for mDia2 on the MT polymer. MT shearing was obtained by passing the MTs through a 26G needle at least 10 times and was confirmed by immunofluorescence. Immunostaining analyses of His-FH1FH2mDia2 were performed in flow chambers in which 2 µM of rhodamine-labeled and taxol-stabilized MTs were immobilized onto coverslips precoated with mutant rigor kinesin (E164A; provided by S. Gilbert, University of Pittsburgh, Pittsburgh, PA) in the presence of 1 mM ATP. Non-specific protein binding to glass surfaces was blocked by 1 mg/ml casein before mDia2 perfusion. 2 µM FH1FH2mDia2 in PEM buffer plus additives (10 µM taxol with an oxygen-scavenging cocktail to prevent photodamage, including 220 µg/ml glucose oxidase, 22.5 mM glucose, 36 µg/ml catalase, and 71.5 mM β-mercaptoethanol) or PEM buffer plus additives alone were then perfused in each chamber and incubated with MTs for 5 min. MTs were then washed three times in PEM buffer plus additives, fixed in 1% glutaraldehyde, and processed for immunofluorescence using mouse anti-His and Cy2 anti–mouse for the detection of FH1FH2mDia2. Preparations were observed using a 60× plan apo objective (1.45 NA) on a TE2000-U microscope. Images were captured with a cooled charge-coupled device camera (Orca ERII) using Metamorph software and figures were assembled with Photoshop.

MT stability assays

PC or DEAE tubulin at 25 µM was induced to polymerize in PEMG buffer with 10% DMSO. Taxol seeds were used in experiments in which the population of surviving MTs was assessed by immunostaining. Polymerization reactions were performed in the presence of 2 µM mDia2 proteins at 37°C for 1 h. To assess MT stability to cold-induced depolymerization, matching aliquots of the samples were centrifuged, as described in the previous section, to isolate the MT pellet. The remaining sample was then incubated at 4°C for 30 min and spun in an ultracentrifuge (TLA100; Beckman Coulter) for 10 min at 60k rpm at 4°C to isolate cold-stable MTs. Samples of the input material, pellets, and supernatants were resolved on 10% SDS-PAGE and the proteins were detected by Coomassie staining. To assess MTs stability to dilution-induced depolymerization, 25 µM DEAE tubulin was polymerized in the presence of taxol seeds to generate longer MTs and recombinant mDia2 fragments at 2 µM were added to MTs diluted 10 times their original volume in PEM buffer (100 mM Pipes-KOH, pH 6.9, 1 mM EGTA, and 2 mM $MgCl_2$) for 10 min at 37°C to induce depolymerization. The reactions were stopped by the addition of 0.5% glutaraldehyde. Matching aliquots of input, diluted, and cold-treated material were then spotted onto polylysine–coated coverslips and fixed by incubating with ice-cold methanol for 5 min. MTs were visualized by staining with a rat anti-Tyr tubulin antibody and a secondary Cy3-conjugated anti–rat antibody and epifluorescence microscopy using a microscope (Optiphot) with a 60× plan apo objective (1.4 NA). Images were captured with a cooled charge-coupled device camera (MicroMax) using Metamorph software and figures were assembled using Photoshop. MT bundling before and after dilution was assessed by polymerizing 25 µM MTs using MT seeds in the presence or absence of 2 µM FH1FH2mDia2. MT bundles were sedimented by low-speed centrifugation at 4,500 *g* for 5 min at room temperature. Matching aliquots of the input materials, pellets, and supernatants were resolved on 10% SDS-PAGE and the proteins were detected by Coomassie staining.

MT dynamics analyses

MT dynamics analyses were performed with MTs nucleated from sea urchin flagellar axoneme fragments and visualized by video-enhanced DIC microscopy as previously described (Walker et al., 1991; Pryer et al., 1992; Howell et al., 1999). In brief, coverslips were mounted on glass slides using double-stick tape as spacers to create a flow chamber of ∼10-µl vol. Sea urchin axonemes were allowed to adhere to the coverslip for 5 min. Chambers were then perfused with 50 µl PEM to remove unbound axonemes and then 5 mg/ml casein to block nonspecific protein binding to glass surfaces. The chamber was then perfused with 50 µl PEM to wash out the casein and finally perfused with a solution of 10 µM tubulin and 1 mM GTP in PEM. In MT assembly reactions to measure MT dynamics, 2 µM His-FH1FH2mDia2 or buffer alone (HKCL + PEM buffer) was added to the MT assembly mixture. The chamber was then warmed on the microscope stage to ∼35°C to initiate MT assembly. In most MT disassembly experiments, a single microscope field was viewed for 2–5 min during assembly and then perfused with either buffer (PEM + HKCL) or solutions containing mDia2 (0.5–4 µM in HKCL). MT growth rates during assembly or before perfusion in MT disassembly experiments were used to define plus and minus ends of the axonemes. Mean rates of elongation and shortening for individual MTs were determined by least squares regression analysis of changes in MT length as a function of time. Frequencies of catastrophe were determined by dividing the total number of catastrophes by the sum of the total time spent in elongation for all MTs of one polarity.

Taxol-stabilized seeds

Taxol-stabilized MT seeds were generated by polymerizing DEAE tubulin at 37°C for 30 min with 100 µM GTP and stepwise addition of Taxol (1–20 µM). MTs were centrifuged at 100,000 *g* for 10 min at 37°C and resuspended in PEM with 100 µM GTP and 20 µM Taxol. Seeds were generated by passing isolated MTs through a 22-gauge syringe 20 times and then isolated by centrifuging at 100,000 *g* for 20 min at 4°C. Pellets were washed twice with PEM and resuspended in half of their initial volume in PEM with 100 µM GTP.

Online supplemental material

Fig. S1 shows that FH1FH2mDia2 stabilizes MTs independently of its tag. Fig. S2 shows that FH1FH2mDia2 bundles MTs in vitro. Fig. S3 shows that FH2C-mDia2 is severely deficient in nucleating actin assembly in vitro. Video 1 shows time lapse of EGFP-FH1FH2mDia2 dynamics in NIH3T3 by TIRF microscopy. Video 2 shows time lapse of W853A EGFP-FH1FH2mDia2 dynamics in NIH3T3 by TIRF microscopy. Video 3 shows time lapse of I704A EGFP-FH1FH2mDia2 dynamics in NIH3T3 by TIRF microscopy. Video 4 shows time lapse of W630A EGFP-FH1FH2mDia2 dynamics in NIH3T3 by TIRF microscopy. Video 5 shows a real-time DIC microscopy video recording of axoneme-nucleated MTs undergoing dilution-induced disassembly in the presence of FH1FH2mDia2. Video 6 shows a real-time DIC microscopy video recording of axoneme-nucleated MTs undergoing dilution-induced disassembly in the presence of HKCL buffer. All movies have been compressed. High-quality uncompressed movies are available upon request. Online supplemental material is available at http://www.jcb.org/cgi/content/full/jcb.200709029/DC1.

We thank Erin Vintinner for outstanding technical assistance, Eric Folker for valuable discussions and Biocore analyses, Ying Wen for GST-APC-C and GST-EB1 proteins, Katia Evans and Brett Lauring for help with gel filtration analyses, and members of the Gundersen laboratory for comments on the manuscript.

This work was supported by National Institutes of Health Grant (GM 62939 to G.G. Gundersen) and a Telethon-Italy Fellowship (GFP03006 to F. Bartolini).

The authors declare that they have no competing financial interests.

Submitted: 5 September 2007
Accepted: 3 April 2008

References

Alberts, A.S. 2001. Identification of a carboxyl-terminal diaphanous-related formin homology protein autoregulatory domain. *J. Biol. Chem.* 276:2824–2830.

Cook, T.A., T. Nagasaki, and G.G. Gundersen. 1998. Rho guanosine triphosphatase mediates the selective stabilization of microtubules induced by lysophosphatidic acid. *J. Cell Biol.* 141:175–185.

Copeland, J.W., and R. Treisman. 2002. The diaphanous-related formin mDia1 controls serum response factor activity through its effects on actin polymerization. *Mol. Biol. Cell.* 13:4088–4099.

Copeland, J.W., S.J. Copeland, and R. Treisman. 2004. Homo-oligomerization is essential for F-actin assembly by the formin family FH2 domain. *J. Biol. Chem.* 279:50250–50256.

Drechsel, D.N., A.A. Hyman, M.H. Cobb, and M.W. Kirschner. 1992. Modulation of the dynamic instability of tubulin assembly by the microtubule-associated protein tau. *Mol. Biol. Cell.* 3:1141–1154.

Eisenmann, K.M., R.A. West, D. Hildebrand, S.M. Kitchen, J. Peng, R. Sigler, J. Zhang, K.A. Siminovitch, and A.S. Alberts. 2007. T cell responses in mammalian diaphanous-related formin mDia1 knock-out mice. *J. Biol. Chem.* 282:25152–25158.

Eng, C.H., T.M. Huckaba, and G.G. Gundersen. 2006. The formin mDia regulates GSK3beta through novel PKCs to promote microtubule stabilization but not MTOC reorientation in migrating fibroblasts. *Mol. Biol. Cell.* 17:5004–5016.

Fernandez-Borja, M., L. Janssen, D. Verwoerd, P. Hordijk, and J. Neefjes. 2005. RhoB regulates endosome transport by promoting actin assembly on endosomal membranes through Dia1. *J. Cell Sci.* 118:2661–2670.

Gasman, S., Y. Kalaidzidis, and M. Zerial. 2003. RhoD regulates endosome dynamics through Diaphanous-related Formin and Src tyrosine kinase. *Nat. Cell Biol.* 5:195–204.

Gomez, T.S., K. Kumar, R.B. Medeiros, Y. Shimizu, P.J. Leibson, and D.D. Billadeau. 2007. Formins regulate the actin-related protein 2/3 complex-independent polarization of the centrosome to the immunological synapse. *Immunity.* 26:177–190.

Goode, B.L., and M.J. Eck. 2007. Mechanism and function of formins in the control of actin assembly. *Annu. Rev. Biochem.* 76:593–627.

Goulimari, P., T.M. Kitzing, H. Knieling, D.T. Brandt, S. Offermanns, and R. Grosse. 2005. Galpha12/13 is essential for directed cell migration and localized Rho-Dia1 function. *J. Biol. Chem.* 280:42242–42251.

Gundersen, G.G., M.H. Kalnoski, and J.C. Bulinski. 1984. Distinct populations of microtubules: tyrosinated and nontyrosinated alpha tubulin are distributed differently in vivo. *Cell.* 38:779–789.

Gundersen, G.G., S. Khawaja, and J.C. Bulinski. 1987. Postpolymerization detyrosination of α-tubulin: a mechanism for subcellular differentiation of microtubules. *J. Cell Biol.* 105:251–264.

Gupton, S.L., K. Eisenmann, A.S. Alberts, and C.M. Waterman-Storer. 2007. mDia2 regulates actin and focal adhesion dynamics and organization in the lamella for efficient epithelial cell migration. *J. Cell Sci.* 120:3475–3487.

Harris, E.S., I. Rouiller, D. Hanein, and H.N. Higgs. 2006. Mechanistic differences in actin bundling activity of two mammalian formins, FRL1 and mDia2. *J. Biol. Chem.* 281:14383–14392.

Higashida, C., T. Miyoshi, A. Fujita, F. Oceguera-Yanez, J. Monypenny, Y. Andou, S. Narumiya, and N. Watanabe. 2004. Actin polymerization-driven molecular movement of mDia1 in living cells. *Science.* 303:2007–2010.

Higgs, H.N., and K.J. Peterson. 2005. Phylogenetic analysis of the formin homology 2 domain. *Mol. Biol. Cell.* 16:1–13.

Ho, C.L., J.L. Martys, A. Mikhailov, G.G. Gundersen, and R.K. Liem. 1998. Novel features of intermediate filament dynamics revealed by green fluorescent protein chimeras. *J. Cell Sci.* 111:1767–1778.

Howell, B., N. Larsson, M. Gullberg, and L. Cassimeris. 1999. Dissociation of the tubulin-sequestering and microtubule catastrophe-promoting activities of oncoprotein 18/stathmin. *Mol. Biol. Cell.* 10:105–118.

Infante, A.S., M.S. Stein, Y. Zhai, G.G. Borisy, and G.G. Gundersen. 2000. Detyrosinated (Glu) microtubules are stabilized by an ATP-sensitive plus-end cap. *J. Cell Sci.* 113:3907–3919.

Ishizaki, T., Y. Morishima, M. Okamoto, T. Furuyashiki, T. Kato, and S. Narumiya. 2001. Coordination of microtubules and the actin cytoskeleton by the Rho effector mDia1. *Nat. Cell Biol.* 3:8–14.

Kato, T., N. Watanabe, Y. Morishima, A. Fujita, T. Ishizaki, and S. Narumiya. 2001. Localization of a mammalian homolog of diaphanous, mDia1, to the mitotic spindle in HeLa cells. *J. Cell Sci.* 114:775–784.

Kodama, A., I. Karakesisoglou, E. Wong, A. Vaezi, and E. Fuchs. 2003. ACF7: an essential integrator of microtubule dynamics. *Cell.* 115:343–354.

Kovar, D.R., J.R. Kuhn, A.L. Tichy, and T.D. Pollard. 2003. The fission yeast cytokinesis formin Cdc12p is a barbed end actin filament capping protein gated by profilin. *J. Cell Biol.* 161:875–887.

Kovar, D.R., E.S. Harris, R. Mahaffy, H.N. Higgs, and T.D. Pollard. 2006. Control of the assembly of ATP- and ADP-actin by formins and profilin. *Cell.* 124:423–435.

Kreitzer, G., G. Liao, and G.G. Gundersen. 1999. Detyrosination of tubulin regulates the interaction of intermediate filaments with microtubules in vivo via a kinesin-dependent mechanism. *Mol. Biol. Cell.* 10:1105–1118.

Leader, B., H. Lim, M.J. Carabatsos, A. Harrington, J. Ecsedy, D. Pellman, R. Maas, and P. Leder. 2002. Formin-2, polyploidy, hypofertility and positioning of the meiotic spindle in mouse oocytes. *Nat. Cell Biol.* 4:921–928.

Li, F., and H.N. Higgs. 2003. The mouse Formin mDia1 is a potent actin nucleation factor regulated by autoinhibition. *Curr. Biol.* 13:1335–1340.

Li, F., and H.N. Higgs. 2005. Dissecting requirements for auto-inhibition of actin nucleation by the formin, mDia1. *J. Biol. Chem.* 280:6986–6992.

Lin, S.X., G.G. Gundersen, and F.R. Maxfield. 2002. Export from pericentriolar endocytic recycling compartment to cell surface depends on stable, detyrosinated (glu) microtubules and kinesin. *Mol. Biol. Cell.* 13:96–109.

Mikhailov, A.V., and G.G. Gundersen. 1995. Centripetal transport of microtubules in motile cells. *Cell Motil. Cytoskeleton.* 32:173–186.

Moseley, J.B., I. Sagot, A.L. Manning, Y. Xu, M.J. Eck, D. Pellman, and B.L. Goode. 2004. A conserved mechanism for Bni1- and mDia1-induced actin assembly and dual regulation of Bni1 by Bud6 and profilin. *Mol. Biol. Cell.* 15:896–907.

Moseley, J.B., S. Maiti, and B.L. Goode. 2006. Formin proteins: purification and measurement of effects on actin assembly. *Methods Enzymol.* 406:215–234.

Otomo, T., C. Otomo, D.R. Tomchick, M. Machius, and M.K. Rosen. 2005. Structural basis of Rho GTPase-mediated activation of the formin mDia1. *Mol. Cell.* 18:273–281.

Palazzo, A.F., T.A. Cook, A.S. Alberts, and G.G. Gundersen. 2001. mDia mediates Rho-regulated formation and orientation of stable microtubules. *Nat. Cell Biol.* 3:723–729.

Palazzo, A.F., C.H. Eng, D.D. Schlaepfer, E.E. Marcantonio, and G.G. Gundersen. 2004. Localized stabilization of microtubules by integrin- and FAK-facilitated Rho signaling. *Science.* 303:836–839.

Pring, M., M. Evangelista, C. Boone, C. Yang, and S.H. Zigmond. 2003. Mechanism of formin-induced nucleation of actin filaments. *Biochemistry.* 42:486–496.

Pruyne, D., M. Evangelista, C. Yang, E. Bi, S. Zigmond, A. Bretscher, and C. Boone. 2002. Role of formins in actin assembly: nucleation and barbed-end association. *Science.* 297:612–615.

Pryer, N.K., R.A. Walker, V.P. Skeen, B.D. Bourns, M.F. Soboeiro, and E.D. Salmon. 1992. Brain microtubule-associated proteins modulate microtubule dynamic instability in vitro. Real-time observations using video microscopy. *J. Cell Sci.* 103:965–976.

Riveline, D., E. Zamir, N.Q. Balaban, U.S. Schwarz, T. Ishizaki, S. Narumiya, Z. Kam, B. Geiger, and A.D. Bershadsky. 2001. Focal contacts as mechanosensors: externally applied local mechanical force induces growth of focal contacts by an mDia1-dependent and ROCK-independent mechanism. *J. Cell Biol.* 153:1175–1186.

Rivero, F., T. Muramoto, A.K. Meyer, H. Urushihara, T.Q. Uyeda, and C. Kitayama. 2005. A comparative sequence analysis reveals a common GBD/FH3-FH1-FH2-DAD architecture in formins from *Dictyostelium*, fungi and metazoa. *BMC Genomics.* 6:28.

Romero, S., C. Le Clainche, D. Didry, C. Egile, D. Pantaloni, and M.F. Carlier. 2004. Formin is a processive motor that requires profilin to accelerate actin assembly and associated ATP hydrolysis. *Cell.* 119:419–429.

Rosales-Nieves, A.E., J.E. Johndrow, L.C. Keller, C.R. Magie, D.M. Pinto-Santini, and S.M. Parkhurst. 2006. Coordination of microtubule and microfilament dynamics by *Drosophila* Rho1, Spire and Cappuccino. *Nat. Cell Biol.* 8:367–376.

Rose, R., M. Weyand, M. Lammers, T. Ishizaki, M.R. Ahmadian, and A. Wittinghofer. 2005. Structural and mechanistic insights into the interaction between Rho and mammalian Dia. *Nature.* 435:513–518.

Rundle, D.R., G. Gorbsky, and L. Tsiokas. 2004. PKD2 interacts and co-localizes with mDia1 to mitotic spindles of dividing cells: role of mDia1 IN PKD2 localization to mitotic spindles. *J. Biol. Chem.* 279:29728–29739.

Sagot, I., A.A. Rodal, J. Moseley, B.L. Goode, and D. Pellman. 2002. An actin nucleation mechanism mediated by Bni1 and profilin. *Nat. Cell Biol.* 4:626–631.

Sakata, D., H. Taniguchi, S. Yasuda, A. Adachi-Morishima, Y. Hamazaki, R. Nakayama, T. Miki, N. Minato, and S. Narumiya. 2007. Impaired T lymphocyte trafficking in mice deficient in an actin-nucleating protein, mDia1. *J. Exp. Med.* 204:2031–2038.

Shimada, A., M. Nyitrai, I.R. Vetter, D. Kuhlmann, B. Bugyi, S. Narumiya, M.A. Geeves, and A. Wittinghofer. 2004. The core FH2 domain of diaphanous-related formins is an elongated actin binding protein that inhibits polymerization. *Mol. Cell.* 13:511–522.

Tian, G., S.A. Lewis, B. Feierbach, T. Stearns, H. Rommelaere, C. Ampe, and N.J. Cowan. 1997. Tubulin subunits exist in an activated conformational state generated and maintained by protein cofactors. *J. Cell Biol.* 138:821–832.

Tominaga, T., E. Sahai, P. Chardin, F. McCormick, S.A. Courtneidge, and A.S. Alberts. 2000. Diaphanous-related formins bridge Rho GTPase and Src tyrosine kinase signaling. *Mol. Cell.* 5:13–25.

Vasquez, R.J., D.L. Gard, and L. Cassimeris. 1994. XMAP from *Xenopus* eggs promotes rapid plus end assembly of microtubules and rapid microtubule polymer turnover. *J. Cell Biol.* 127:985–993.

Vavylonis, D., D.R. Kovar, B. O'Shaughnessy, and T.D. Pollard. 2006. Model of formin-associated actin filament elongation. *Mol. Cell.* 21:455–466.

Walker, R.A., N.K. Pryer, and E.D. Salmon. 1991. Dilution of individual microtubules observed in real time in vitro: evidence that cap size is small and independent of elongation rate. *J. Cell Biol.* 114:73–81.

Wallar, B.J., A.D. Deward, J.H. Resau, and A.S. Alberts. 2007. RhoB and the mammalian Diaphanous-related formin mDia2 in endosome trafficking. *Exp. Cell Res.* 313:560–571.

Watanabe, N., T. Kato, A. Fujita, T. Ishizaki, and S. Narumiya. 1999. Cooperation between mDia1 and ROCK in Rho-induced actin reorganization. *Nat. Cell Biol.* 1:136–143.

Wen, Y., C.H. Eng, J. Schmoranzer, N. Cabrera-Poch, E.J. Morris, M. Chen, B.J. Wallar, A.S. Alberts, and G.G. Gundersen. 2004. EB1 and APC bind to mDia to stabilize microtubules downstream of Rho and promote cell migration. *Nat. Cell Biol.* 6:820–830.

Xu, Y., J.B. Moseley, I. Sagot, F. Poy, D. Pellman, B.L. Goode, and M.J. Eck. 2004. Crystal structures of a Formin Homology-2 domain reveal a tethered dimer architecture. *Cell.* 116:711–723.

Yamana, N., Y. Arakawa, T. Nishino, K. Kurokawa, M. Tanji, R.E. Itoh, J. Monypenny, T. Ishizaki, H. Bito, K. Nozaki, et al. 2006. The Rho-mDia1 pathway regulates cell polarity and focal adhesion turnover in migrating cells through mobilizing Apc and c-Src. *Mol. Cell. Biol.* 26:6844–6858.

Yasuda, S., F. Oceguera-Yanez, T. Kato, M. Okamoto, S. Yonemura, Y. Terada, T. Ishizaki, and S. Narumiya. 2004. Cdc42 and mDia3 regulate microtubule attachment to kinetochores. *Nature.* 428:767–771.